Abderrahmane LAKIKZA [1], Hocine CHEGHIB [1], Nabil KAHOUL [1]

# Optimized variational mode decomposition for improved bearing fault diagnosis and performance evaluation

This research presents an enhanced methodology for diagnosing bearing faults using Variational Mode Decomposition (VMD) based on L-Kurtosis analysis. The proposed method focuses on selecting optimal parameters for VMD to extract the mode containing the most information related to the fault. The selection of these parameters is based on comparing the energy ratio of each mode and the absolute difference in L-Kurtosis between the Intrinsic Mode Function (IMF) with the highest energy and the original signal. The extracted mode is further refined using a specified kurtosis rate threshold to ensure the most relevant significant modes are captured. The proposed methodology was tested using real fault data from the CWRU, XJTUSY, and a real-world wind turbine dataset related to electric motors and wind turbine systems. The results demonstrated high accuracy in fault detection compared to other methods such as the Gini Index, correlation, and traditional decomposition techniques like EMD (Empirical Mode Decomposition). Furthermore, due to the simple computational nature of the improved VMD method, it is faster and more efficient compared to methods that rely on complex calculations or frequency band analysis, making it suitable for applications requiring real-time, reliable fault diagnosis.

## Nomenclature

VMD  Variational Mode Decomposition
$\alpha$     Penalty factor used in VMD
$K$     Number of modes in VMD
$F$     Frequency
E     Energy
IMF   Intrinsic Mode Function
EMD   Empirical Mode Decomposition

✉ Abderrahmane LAKIKZA, e-mail: abderrahmane.lakikza@univ-annaba.dz

[1]Electromechanical Systems Laboratory, Badji Mokhtar-Annaba University, Annaba, Algeria

EEMD    Ensemble Empirical Mode Decomposition
GI      Gini index
*Lk*    L-Kurtosis
*Ku*    Kurtosis
FSST    Fourier Synchro Squeezed Transform
FBE     Frequency Band Analysis
GA      Genetic Algorithm
KEMI    Kernel-based Mutual Information
SR      Stochastic Resonance
CWRU    Case Western Reserve University
XJTU-SY Xi'an Jiaotong University – Shaanxi Yanchang dataset

## 1. Introduction

Bearings are critical components in rotating machinery and wind turbine systems, playing a significant role in maintaining the continuous and stable operation of these systems [1]. With the increasing reliance on wind energy as a primary source of renewable energy, they have become one of the most important energy sources worldwide, ranking second only to solar energy in their contribution to global electricity supply [2]. According to the International Energy Agency, there have been significant advancements in wind energy technology in recent years [3]. However, the maintenance and operational costs of wind turbines remain high [4], necessitating a focus on monitoring systems, performance enhancement, fault diagnosis, and preventive maintenance to ensure continuous production. Faults in wind turbines vary based on the specific components involved, with all types of turbines sharing blades and nacelles that play a crucial role in converting wind energy into electrical power. Therefore, the nacelle underscores the importance of the operational health of critical components such as the generator, gearbox, main bearings, and rotor shaft [5].

The methods and approaches for fault diagnosis vary based on different types of data, objectives, and capabilities. Effective fault detection is essential for achieving operational efficiency and reducing unplanned downtime. In this context, recent years have witnessed significant advancements in machine learning techniques, such as Support Vector Machine [6–8] and Artificial Neural Networks [7], along with advanced signal analysis techniques like Variational Mode Decomposition [9], greatly enhancing maintenance and diagnostic processes in wind turbine and rotating machinery systems.

Given the importance of ensuring bearing health, as various failures can cause significant damage to wind turbine and rotating machinery components [10], the primary goal of this study is to develop effective techniques for early and accurate bearing fault diagnosis. Early fault detection will contribute to improved operational efficiency and reduced costs associated with unplanned maintenance in wind turbine and rotating machinery systems. Signal processing methods play a significant

role in this process, utilizing advanced techniques to analyze data from bearing performance. These methods employ mathematical tools tailored for analyzing non-stationary and non-linear signals, such as EMD, EEMD, and VMD [10], in addition to frequency and time-domain analysis techniques. VMD, known for its effectiveness, has seen a diversity in parameter tuning algorithms and the selection of appropriate modes in previous studies, aiming for more precise analysis of bearing conditions [10–17].

Furthermore, traditional signal processing methods aim to eliminate noise from signals to reveal fault characteristics, yet Stochastic Resonance [18] offers a different approach by leveraging the noise within signals to enhance the detection of weak fault features. SR has been extensively applied in machinery fault detection, particularly for critical rotary components such as rolling element bearings, gears, and rotors. Recent studies highlight the growing importance of SR in this field, providing valuable insights and laying the groundwork for future research endeavors [18].

One of the prominent studies in this field [10] has introduced an original method based on the criterion of the maximum value of envelope kurtosis to optimize and determine the mode number in the VMD method. This method effectively solves the problem of needing to predetermine the mode number. Additionally, a novel methodology was presented to select the sensitive Intrinsic Mode Functions containing abundant fault information based on the Frequency Band Energy analysis.

This study [11] presents an adaptive framework utilizing Variational Mode Decomposition to enhance fault diagnosis in rolling bearings by optimizing the selection of decomposition parameters. To achieve this, the Sailfish Optimization algorithm was integrated with the Gini Index as a criterion for selecting the optimal modes, thereby aiding in noise reduction and the extraction of faultrelevant information. The results demonstrate that the proposed method significantly improves the accuracy of fault feature extraction, outperforming traditional methods such as fixed-parameter VMD, Local Mean Decomposition, and Ensemble Empirical Mode Decomposition.

In the last three stages of the proposed methodology in this paper [12] the optimal modes were discussed using the kurtosis criterion, where the signal was reconstructed with the IMFs that have higher than average kurtosis. In the final section of this work [13], the weighted kurtosis was utilized to extract the optimal mode, which relies on the kurtosis index and correlation with the original signal. A novel methodology was proposed in this paper [14] to enhance the Variable Mode Decomposition technique using the maximum kurtosis criterion to address the issue of pre-determining parameters. This method focuses on optimizing the value of (K) first, and then optimizing the penalty factor value based on the optimal (K), significantly improving the method's performance. Additionally, the study suggested a new approach for selecting sensitive Intrinsic Mode Functions based on resonant frequency. Using the power spectrum, the resonant frequency for both

the original signal and each IMF is identified, and these frequencies are compared to select the most sensitive IMF for fault detection.

In the paper [17], a genetic algorithm and kernel-based mutual information fitness function were used to optimize Variational Mode Decomposition for bearing fault detection. The study employed Fourier synchro squeezed transform to extract instantaneous frequency and convert time-domain signals into the angular domain for identifying defects at varying speeds. Despite the accuracy of the method, the complexity of the computations involved with GA and KEMI presents challenges for applications requiring high-speed processing.

In our research, we aim to develop a new comprehensive and more effective method for bearing fault detection by using kurtosis, L-Kurtosis, and the energy ratio in the modes. This method will be applied to various fault cases and compared with other works as mentioned in the literature review of previous studies.

## 2. Methods

### 2.1. Variational Mode Decomposition

The Variational Mode Decomposition is a modern technique for analyzing non-stationary signals and decomposing them into different frequency components called modes. This method was developed by K. Dragomiretskiy and D. Zosso in 2013 [15]. The VMD algorithm aims to enhance the performance of traditional methods like EMD by offering a non-recursive variational model. VMD simultaneously extracts modes, which improves efficiency and accuracy in handling noise and irregular samples.

In VMD, the signal $f(t)$ is represented as a sum of intrinsic mode functions $u_k(t)$.

$$f(t) = \sum_{k=1}^{K} u_k(t). \tag{1}$$

The VMD method decomposes the signal into several IMFs, each characterized by specific central frequencies and narrow bandwidths. This is achieved using principles from Hilbert transform and frequency mixing, making VMD particularly effective for preprocessing nonlinear signals [8]. The core of the VMD algorithm involves solving an optimization problem to minimize the bandwidth of all modes. The goal is to find the modes $u_k(t)$ and their associated central frequencies $\omega_k$ such that the sum of their bandwidths is minimized. The cost function used in this optimization is [15]:

$$\min_{\{u_k\}, \{\omega_k\}} \left\{ \sum_k \left\| \partial_t \left[ \left( \delta(t) + \frac{i}{\pi t} \right) u_k(t) \right] e^{-\omega_k t} \right\|_2^2 \right\}, \tag{2}$$

where $\partial_t$ is the time derivative.

To optimize the cost function, the Alternating Direction Method of Multipliers (ADMM) is used. The Lagrangian of the problem is defined as [15]:

$$
L(\{u_k\}, \{\omega_k\}, \lambda) = \alpha \sum_k \left\| \partial_t \left[ \left( \delta(t) + j\frac{\partial}{\partial t} \right) u_k(t) \right] e^{-j\omega_k t} \right\|^2
$$
$$
+ \left\| f(t) - \sum_k u_k(t) \right\|^2,
\tag{3}
$$

where $\lambda$ is the Lagrange multiplier and the solution steps are:

- the modes $u_k(t)$ and the center frequencies $\omega_k$ are updated simultaneously until convergence;
- the Lagrange multiplier $\lambda$ is adjusted to ensure constraints are met.

To implement and analyze the VMD technique, the MATLAB programming environment was used. MATLAB provides powerful tools for signal analysis and handling the complex calculations required to apply the VMD technique. The VMD algorithm is executed in MATLAB using custom code that analyzes the signal and extracts the desired modes according to the mathematical equations outlined above.

## 2.2. L-Kurtosis

L-Kurtosis is an advanced statistical indicator used to analyze data and estimate the degree of kurtosis in data distributions [19]. It represents an evolution from traditional kurtosis measures, providing accurate and stable estimations that enhance analytical and diagnostic capabilities [19]. Widely used in fault diagnosis such as bearing faults [19, 20], particularly in fields requiring detection of unusual or abnormal changes in data behavior, L-Kurtosis facilitates the selection of optimal Intrinsic Mode Functions containing information indicative of bearing faults, as demonstrated in the study [20].

To calculate L-Kurtosis, follow these steps:

First, we need to compute the internal orders (L-moments) of the distribution. Internal orders are estimations of distribution parameters using order statistics from the data.

Given a sample of size $q$ from a continuous random variable, denoted by $u_1$, $u_2, \ldots, u_q$, the order statistics are the values sorted in ascending order. These are often denoted as $u_{1:q}, u_{2:q}, \ldots, u_{q:q}$.

L-moments are linear combinations of order statistics. They provide a robust and intuitive measure of the shape of a distribution. The $r$-th L-moment $lm_r$ is defined using the expectation of these order statistics [18]. The $r$-th L-moment $lm_r$ is given by:

$$
lm_r = \frac{1}{r} \sum_{k=0}^{r-1} (-1)^k \binom{r-1}{k} E[u_{r-k:r}],
\tag{4}
$$

where:

$E[u_{r-k:r}]$ is the expectation of the $(r-k)$-th order statistic from a sample of size $r$,

$\begin{pmatrix} r-1 \\ k \end{pmatrix}$ is the binomial coefficient.

- First L-moment: Defined as the average value of the distribution.

$$lm_1 = E[u] = \int_0^1 u \, dF(u). \tag{5}$$

- Second L-moment:

$$lm_2 = \frac{1}{2} E[u_{2:2} - u_{1:2}] = \int_0^1 u(2F(u) - 1) \, dF(u). \tag{6}$$

- Third L-moment:

$$lm_3 = \frac{1}{3} E[u_{3:3} - 2u_{2:3} + u_{1:3}] = \int_0^1 u\left(6F^2(u) - 6F(u) + 1\right) dF(u). \tag{7}$$

- Fourth L-moment:

$$lm_4 = \frac{1}{3} E[u_{4:4} - 3u_{3:4} + 3u_{2:4} - u_{1:4}]$$

$$= \int_0^1 u\left(20F^3(u) - 30F^2(u) + 12F(u) + 1\right) dF(u), \tag{8}$$

$$Lk = \frac{lm_4}{lm_2}. \tag{9}$$

Where we use a discrete sample $x_1, x_2, \ldots, x_N$ of size $N$, we sort the data in ascending order to obtain the order statistics $x_{1:N} \leqslant x_{2:N} \leqslant \ldots \leqslant x_{N:N}$.

$$Lk = \frac{L_4}{L_2}, \tag{10}$$

where:

$$\begin{aligned} L_1 &= \beta_0 \,, \\ L_2 &= 2\beta_1 - \beta_0 \,, \\ L_3 &= 6\beta_2 - 6\beta_1 + \beta_0 \,, \\ L_4 &= 20\beta_3 - 30\beta_2 + 12\beta_1 - \beta_0 \,. \end{aligned} \tag{11}$$

The weighted moments $\beta_i$ for the discrete data are calculated as follows:

$$
\begin{aligned}
\beta_0 &= \frac{1}{N} \sum_{i=1}^{N} x_i, \\
\beta_1 &= \frac{1}{N} \sum_{i=2}^{N} x_i \left( \frac{i-1}{N-1} \right), \\
\beta_2 &= \frac{1}{N} \sum_{i=3}^{N} x_i \left( \frac{(i-1)(i-2)}{(N-1)(N-2)} \right), \\
\beta_3 &= \frac{1}{N} \sum_{i=4}^{N} x_i \left( \frac{(i-1)(i-2)(i-3)}{(N-1)(N-2)(N-3)} \right).
\end{aligned}
\tag{12}
$$

L-Kurtosis is preferred over traditional kurtosis because it offers greater robustness to noise, reduces the impact of outliers, and provides better differentiation between different types of distributions.

### 2.3. Energy ratio and traditional kurtosis

Let's assume we have a signal $x[n]$ and we decompose it using VMD, resulting in IMFs. The energy ratio for each intrinsic mode is calculated as follows:

$$
\begin{aligned}
Energy\ Ratio_i &= \frac{E_i}{E_{\text{total}}}, \\
E_{\text{total}} &= \sum_{n=0}^{N-1} |x[n]|^2, \\
E_i &= \sum_{n=0}^{N-1} |\text{IMF}_i[n]|^2,
\end{aligned}
\tag{13}
$$

where: $Energy\ Ratio_i$ is the energy ratio of the intrinsic mode function $\text{IMF}_i$, $E_{\text{total}}$ is the total energy of the original signal, $E_i$ is the total energy of the intrinsic mode function $\text{IMF}_i$, $N$ is the total number of samples in the intrinsic mode function.

The traditional kurtosis is calculated as follows:

$$
Ku = \frac{1}{N} \frac{\sum_{n=1}^{N} (x(n) - \bar{x})^4}{\left[ \left( \frac{1}{N} \right) \sum_{n=1}^{N} (x(n) - \bar{x})^2 \right]^2},
\tag{14}
$$

where: $N$ – sample size, $x(n)$ – samples, $\bar{x}$ – mean.

### 2.4. The proposed methods

Fig. 1 illustrates the approach used to determine the optimal value of $\alpha$. We explain the algorithm in these steps:

1. Input the original signal

$$x(t). \tag{15}$$

2. Compute the L-Kurtosis of the original signal

$$Lk\big(x(t)\big). \tag{16}$$

3. Define the number of components $K$, define the range of $\alpha$ values from $a$ to $b$

$$K, \; \alpha \in [a, \, b]. \tag{17}$$

4. Set the initial $\alpha$ to $a$

$$\alpha = a. \tag{18}$$

5. Perform VMD using the current value of $\alpha$ to obtain IMFs

$$\text{VMD}\big(x(t), \, \alpha, \, K\big) = [\text{IMFs} + \text{res}]. \tag{19}$$

6. Identify the IMF with the highest energy.

$$\text{IMF}_{\text{max\_energy}} . \tag{20}$$
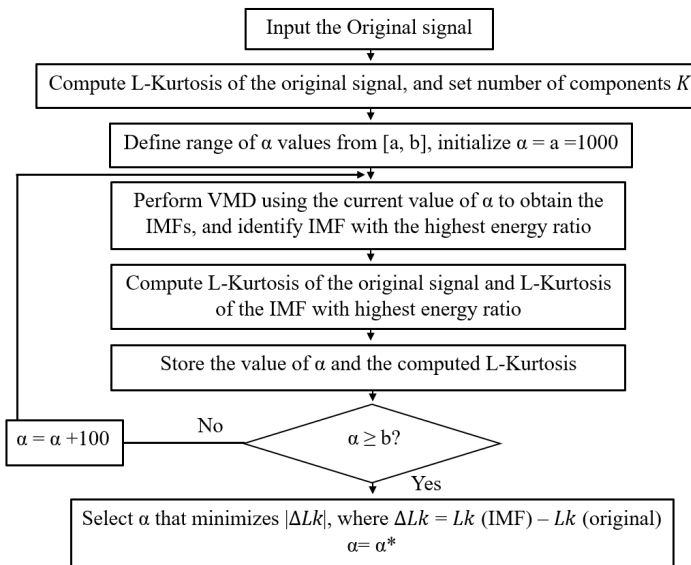


Fig. 1. The proposed algorithm of alpha optimization

7. Compute the L-Kurtosis of the IMF with the highest energy, store the value of $\alpha$ and the computed L-Kurtosis

$$Lk(\text{IMF}_{\text{max\_energy}}), \ \text{store}(\alpha, \ Lk(\text{IMF}_{\text{max\_energy}})). \tag{21}$$

8. Check if $\alpha < b$: Increase $\alpha$ by 100 and repeat steps 5 to 8

$$\alpha = \alpha + 100. \tag{22}$$

If $\alpha \geq b$, proceed to step 9.

The choice of increasing (alpha) in steps of 100 balanced computational efficiency with the need to explore a broad range of values. This step size effectively identified an appropriate (alpha) without imposing a heavy computational burden, enhancing fault feature extraction and mode analysis. While smaller steps could offer greater precision, they would significantly increase computation time. Thus, a step size of 100 was selected to provide a good trade-off between accuracy and efficiency.

9. Select the value of $\alpha$ where the L-Kurtosis of the IMF with the highest energy is closest to the L-Kurtosis of the original signal.

$$\alpha_{\text{optimal}} = \arg \min_{\alpha} \left| Lk\left(\text{IMF}_{\text{max\_energy}}\right) - Lk_{\text{original}} \right|. \tag{23}$$

Fig. 2 demonstrates the second section, which represents the proposed approach to find the optimal number of components $K$ for the VMD that minimizes the energy differences between consecutive IMFs. Then, we select the optimal mode using the kurtosis and L-Kurtosis.

**Step 1:** Set $K$ values from $c$ to $d$, after we start with $K = c$:

$$K \in \{c, \ c+1, \ \ldots, \ d\}. \tag{24}$$

**Step 2:** Decompose the signal $x[n]$ using $\alpha$ optimal and current $K$:

$$[\text{IMFs} + \text{res}] = \text{VMD}\big(x[n] \, \alpha_{\text{optimal}}, \ K\big). \tag{25}$$

**Step 3:** Calculate and sort energies $E_i$ and compute energy differences between consecutive IMFs (ranked in descending order of energy ratio) and record maximum energy difference $\Delta E_{\text{max}}$

$$\Delta E_i = \left| E_i - E_{i+1} \right|. \tag{26}$$

**Step 4:** Store $K$ and $\Delta E_{\text{max}}$, increment $K$ by 1 and repeat step 2–4 until $K$ reaches $d$, then we choose $K$ with the smallest $\Delta E_{\text{max}}$.

**Step 5:** Perform VMD using $\alpha_{\text{optimal}}$ and $K_{\text{optimal}}$ and obtain IMFs $(\text{IMF}_1 \ldots \text{IMF}_k)$.
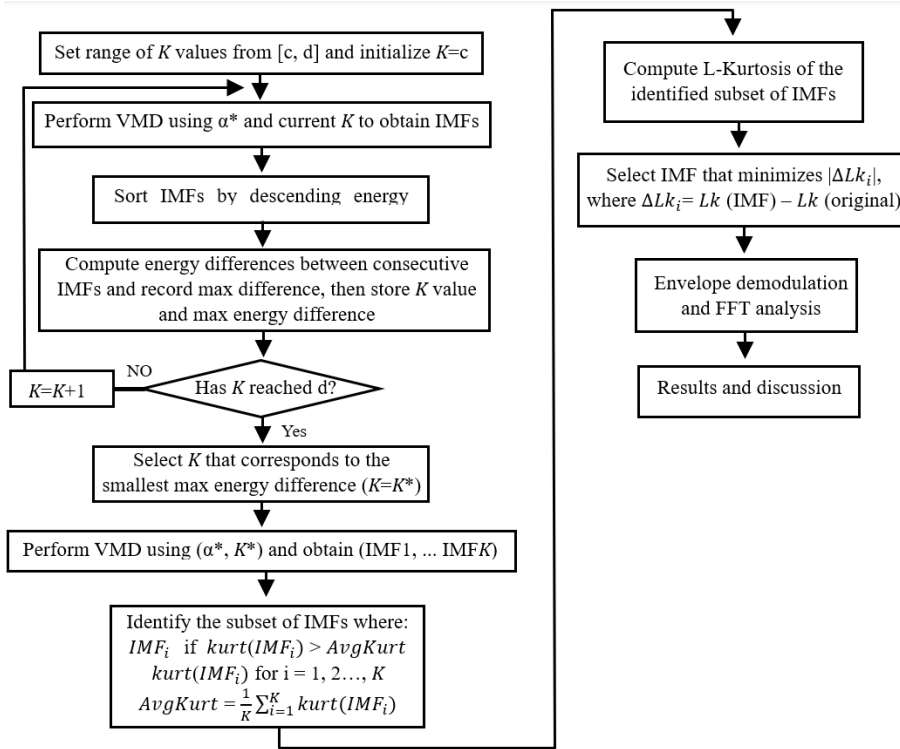
Fig. 2. Process flow for determining optimal K and selecting the optimal IMF

**Step 6:** Calculate the average kurtosis and identify the subset of IMFs whose kurtosis is higher than the average kurtosis.

$$\text{AvgKurt} = \frac{1}{K} \sum_{i=1}^{K} Ku(\text{IMF}_i). \tag{27}$$

**Step 7:** Calculate the L-Kurtosis of the identified subset, then we select the mode whose L-Kurtosis is closest to the L-Kurtosis of the original signal.

The bearing defect frequencies are calculated using the following formulas [10]:

$$Fi = \frac{n}{2}\frac{N}{60}\left(1 + \frac{d}{D}\cos\beta\right), \tag{28}$$

$$Fo = \frac{n}{2}\frac{N}{60}\left(1 - \frac{d}{D}\cos\beta\right), \tag{29}$$

$$Fb = \frac{n}{2d}\frac{N}{60}\left(1 - \left(\frac{d}{D}\cos\beta\right)^2\right), \tag{30}$$

$$Fc = \frac{N}{120}\left(1 - \frac{d}{D}\cos\beta\right).$$  (31)

where: $N$ – rational speed of the rotor, $d$ – diameter of ball, $D$ – pitch diameter, $n$ – number of rolling elements, $\beta$ – angle of contact.

# 3. Results and discussion

## 3.1. Analysis of inner race bearing fault from CWRU database

The simulation model is a signal of a bearing inner race fault from the laboratory of Case Western Reserve University [21], the information of the bearing and fault characteristics is provided in Table 1.

Table 1. Characteristics of the defect and vibrational signal

| Component | Drive end bearing 6205-2RS JEM SKF |
|---|---|
| Operating speed | 1797 rmp |
| Sampling frequency | 12000 Hz |
| Defect diameter | 0.7112 mm |
| Inner race fault frequency | 162.2 Hz |

Experiments were conducted using a 2 hp Reliance Electric motor, and acceleration data was measured [21].

Fig. 3 shows the signal in the time domain. We define the range alpha [1000, 2000] and set $K = 3$. The first partition yielded the results shown in Fig. 4, and the results of the energy ratio for each mode were as follows:

- *Energy Ratio$_1$* = 0.593.
- *Energy Ratio$_2$* = 0.185.
- *Energy Ratio$_3$* = 0.206.

After calculating the difference between the L-Kurtosis of the mode with the highest energy and the original signal for different values of alpha, the results indicated that the optimal $\alpha$ value was 1100. The results are shown in Fig. 5.
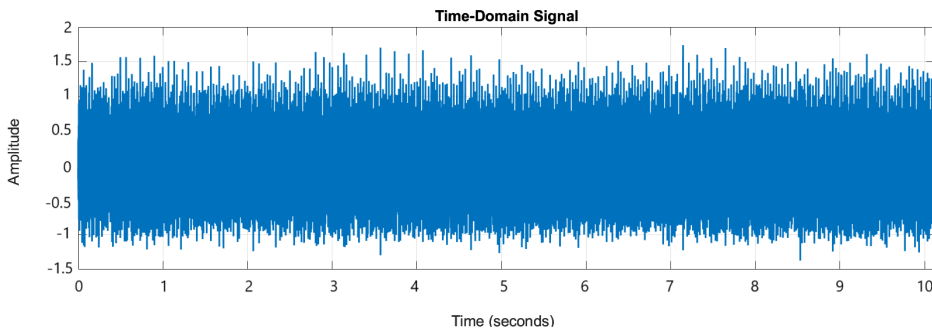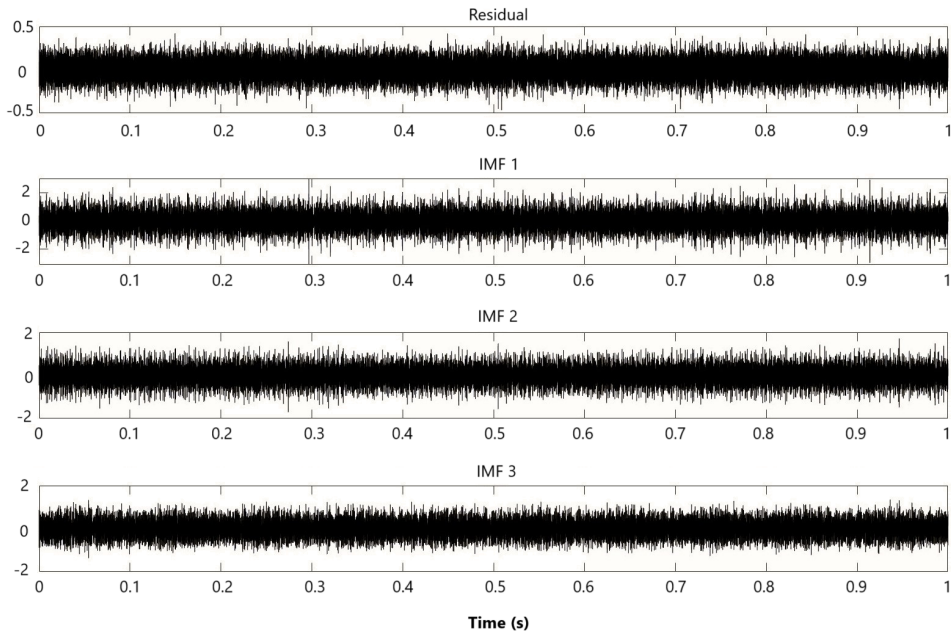


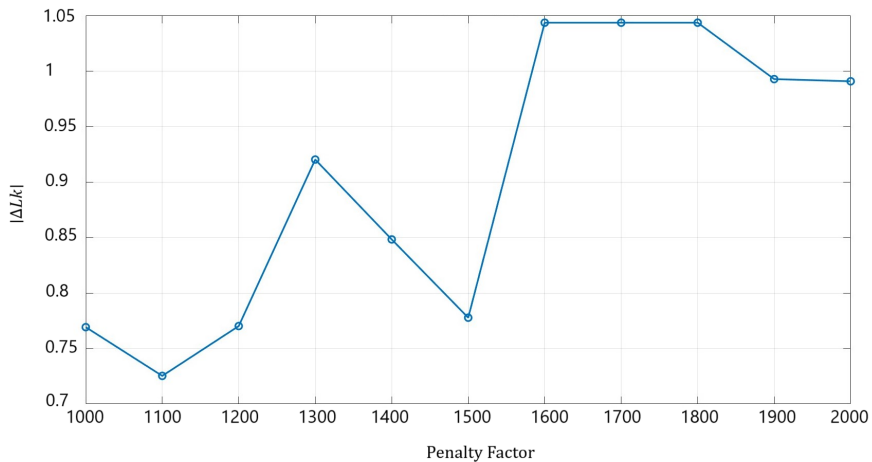Fig. 3. Time domain analysis

Fig. 4. Variational mode decomposition



Fig. 5. Evolution of $|\Delta Lk|$ with different alpha values

After ranking the IMFs according to their energy ratio, we define the differences between the energies of successive IMFs as described in formula (25).

We define the number of modes $K$ from [3, 10]. For each value of $K$ we calculate the $\Delta E_i$ as below (Table 2).

Table 2 indicates the proposed approach results in an optimal $(K)$ value of 8. The VMD results with the optimal alpha and $K$ are shown in Fig. 6. Afterward, we

Table 2. Overview of $\Delta E_i$ values for different $(K)$ after sorting IMFs by energy ratio

| $K$ \ $E_i$ | $\Delta E_1$ | $\Delta E_2$ | $\Delta E_3$ | $\Delta E_4$ | $\Delta E_5$ | $\Delta E_6$ | $\Delta E_7$ | $\Delta E_8$ | $\Delta E_9$ |
|---|---|---|---|---|---|---|---|---|---|
| 3 | **0.375** | 0.0029 | * | * | * | * | * | * | * |
| 4 | **0.334** | 0.0281 | 0.0166 | * | * | * | * | * | * |
| 5 | 0.0636 | 0.0427 | **0.0748** | 0.0168 | * | * | * | * | * |
| 6 | 0.0680 | **0.0762** | 0.0532 | 0.0079 | 0.0737 | * | * | * | * |
| 7 | **0.1696** | 0.0001 | 0.0509 | 0.0139 | 0.0065 | 0.0562 | * | * | * |
| **8** | 0.0326 | **0.0345** | 0.052 | 0.0151 | 0.0111 | 0.02 | 0.0311 | * | * |
| 9 | 0.0184 | 0.0297 | 0.0075 | 0.0165 | 0.0160 | **0.0354** | 0.0139 | 0.0137 | * |
| 10 | **0.0459** | 0.0009 | 0.0080 | 0.0342 | 0.0126 | 0.0204 | 0.0045 | 0.0038 | 0.0153 |

calculate the kurtosis and L-Kurtosis for each IMF and identify the optimal IMF according to the proposed algorithm.
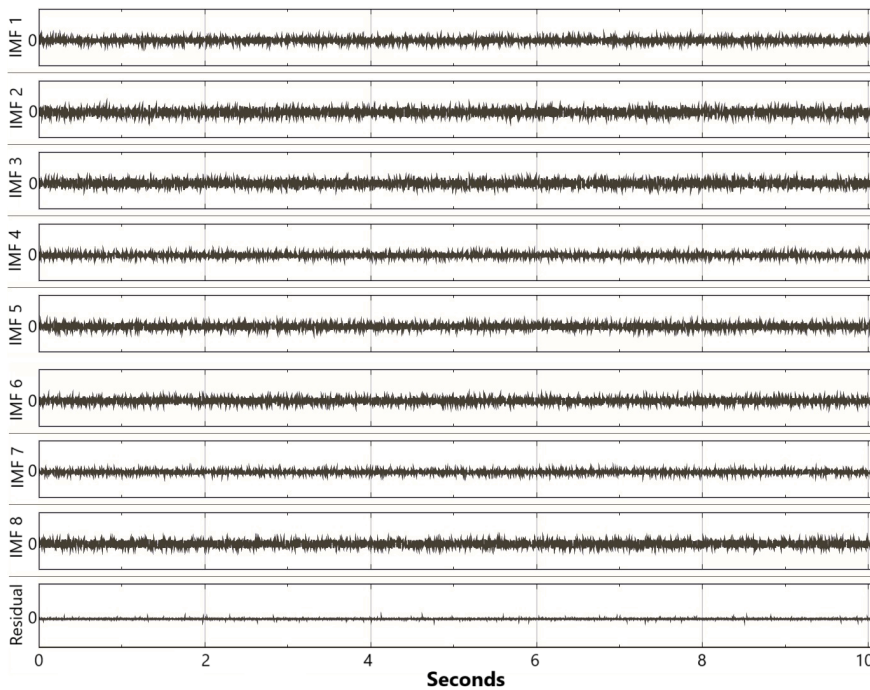


Fig. 6. The optimized VMD results of the inner race fault

The average kurtosis of IMFs is AvgKurt = 2.987 and the L-Kurtosis of the original signal is $Lk = -0.2386$. Based on the results shown in Table 3, the optimal mode is IMF6.

From Table 3, we observe that the kurtosis indicates that the optimal mode is IMF7, while the correlation suggests that the optimal mode is IMF2. Fig. 7 shows

Table 3. Evaluation of Statical measure for optimal IMF selection

| IMFs Measure | IMF1 | IMF2 | IMF3 | IMF4 | IMF5 | IMF6 | IMF7 | IMF8 |
|---|---|---|---|---|---|---|---|---|
| Kurtosis | 2.975 | 2.939 | **3.248** | 2.977 | 2.858 | **3.140** | **3.399** | 2.361 |
| L-Kurtosis | 0.373 | 0.501 | –2.07 | 0.422 | 0.690 | **0.397** | 0.876 | –1.47 |
| Correlation | 0.368 | 0.554 | 0.519 | 0.311 | 0.326 | 0.348 | 0.269 | 0.399 |

the results of the Envelope Spectrum for each mode, demonstrating the superiority of the proposed methodology in accurately detecting the fault.
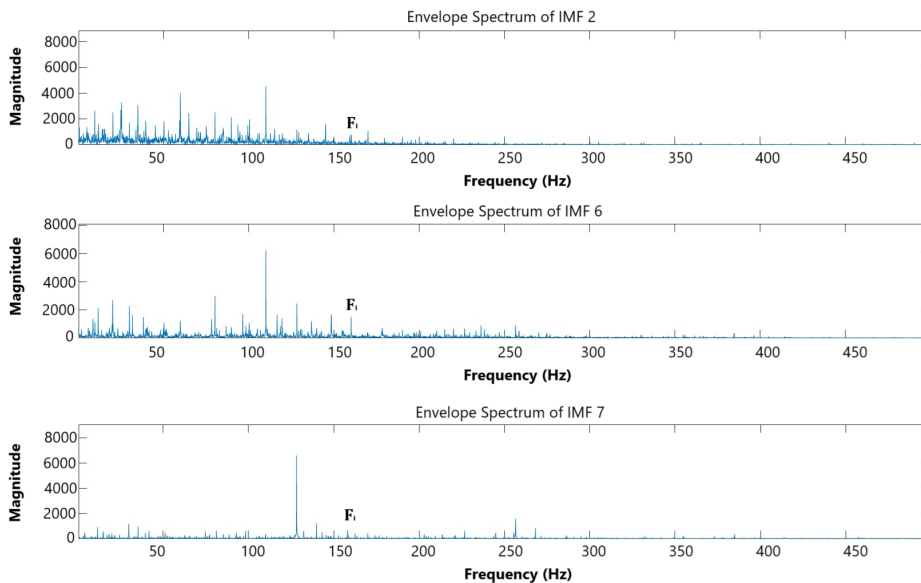


Fig. 7. Envelope spectra of IMF2, IMF6 and IMF7

## 3.2. Analysis of bearing ball fault from CWRU database

We use the proposed approach of VMD to analyze the condition of the bearing 6205-2RS JEM SKF located at the drive end. The technical characteristics of the data are shown in Table 4.

Table 4. The detailed specification of the bearing

| File name | 118.m |
|---|---|
| Operating speed | 1797 rmp |
| Sampling frequency | 12 000 Hz |
| Defect diameter | 0.178 mm |
| Fault frequency | 140.5 Hz |

The vibration signal of the fault prior to VMD analysis yielded the results shown in Fig. 8 and Fig. 9, where the extracted fault information was accompanied by noise. Therefore, the proposed VMD method is used to address this issue.
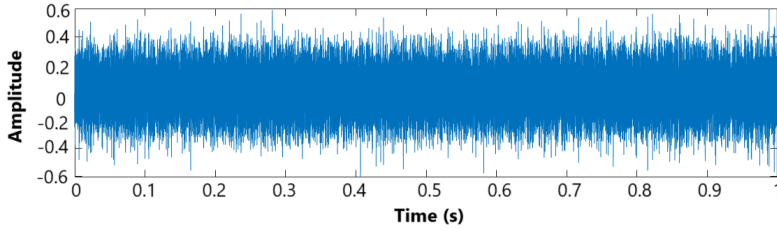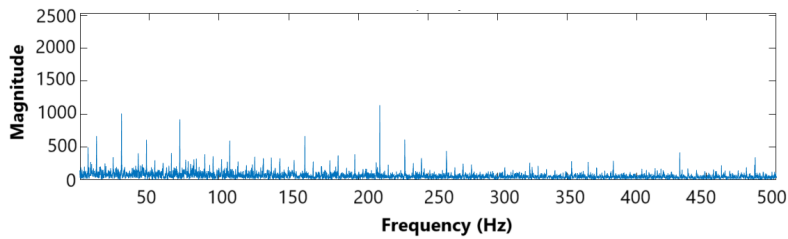


Fig. 8. Time domain analysis



Fig. 9. Frequency domain analysis

We start by setting $K = 3$ and defining the alpha range [1000, 2000].

The proposed algorithm was applied to calculate the L-Kurtosis of the original signal and determine the optimal range of $\alpha$ values. Fig. 10 showing the variation of $|\Delta Lk|$ with respect to $\alpha$ indicates that the optimal value of $\alpha$ is 1900. This result implies that $\alpha = 1900$ is the value that achieves the closest L-Kurtosis between the
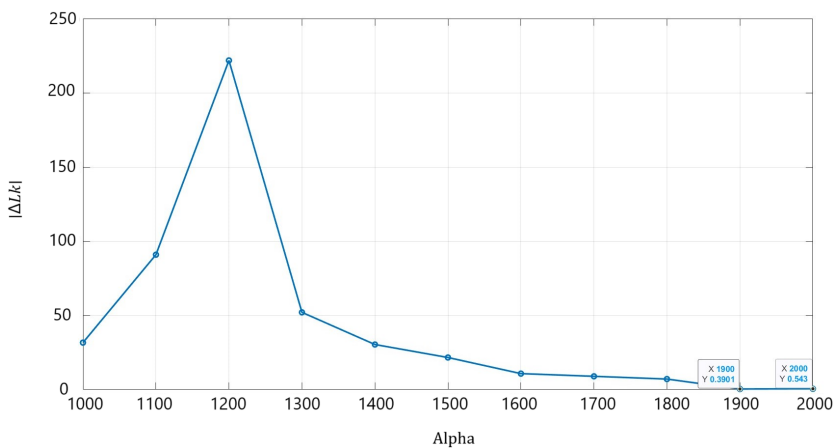


Fig. 10. Evolution of $|\Delta Lk|$ with respect to the alpha values

IMF with the highest energy ratio and the L-Kurtosis of the original signal. The reduction in $|\Delta Lk|$ suggests that the IMF extracted using $\alpha = 1900$ more accurately reflects the statistical properties of the original signal. After determining the optimal $\alpha$, the signal was decomposed in several trials using different values of $K$ within the specified range [3, 10]. The energy differences between consecutive IMFs were calculated, and the maximum difference for each trial of $K$ was recorded. Table 5 below presents the results of the energy differences between consecutive IMFs for all tested $K$ values, showing that the optimal $K$ is IMF5:

Table 5. Energy differences between extracted (IMFs) for various $K$ values

| $\Delta E_i$ / $K$ | $\Delta E_1$ | $\Delta E_2$ | $\Delta E_3$ | $\Delta E_4$ | $\Delta E_5$ | $\Delta E_6$ | $\Delta E_7$ | $\Delta E_8$ | $\Delta E_9$ |
|---|---|---|---|---|---|---|---|---|---|
| 3 | **0.815** | 0.0114 | * | * | * | * | * | * | * |
| 4 | **0.478** | 0.155 | 0.025 | * | * | * | * | * | * |
| 5 | 0.0505 | **0.136** | 0.130 | 0.0274 | * | * | * | * | * |
| 6 | 0.0109 | **0.201** | 0.063 | 0.0136 | 0.0278 | * | * | * | * |
| 7 | 0.0149 | **0.187** | 0.0366 | 0.0248 | 0.0047 | 0.0235 | * | * | * |
| 8 | 0.0159 | **0.2118** | 0.0079 | 0.0205 | 0.0008 | 0.0278 | 0.0011 | * | * |
| 9 | 0.0096 | **0.1926** | 0.0181 | 0.0005 | 0.0246 | 0.0094 | 0.0126 | 0.0131 | * |
| 10 | 0.007 | **0.1373** | 0.0317 | 0.014 | 0.0142 | 0.0064 | 0.0152 | 0.0062 | 0.0126 |

After determining the optimal values of $\alpha = 1900$ and $K = 5$, the signal was decomposed using VMD with these parameters. The following figure (Fig. 11) illustrates the results of this decomposition.
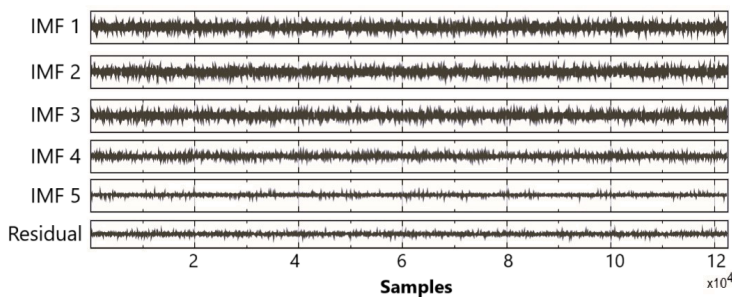


Fig. 11. The optimized VMD results of the ball fault

Several properties of the modes were evaluated, including kurtosis, L-Kurtosis, correlation, and the Gini index given by the following expression [11]:

$$GI(x) = 1 - 2 \sum \frac{|x_{[k]}|}{x_1} \times \left( \frac{N - k + 0.5}{N} \right), \tag{32}$$

considering a vector $x = \left[x(1), \ldots, x(N)\right]$, where its elements are reordered and denoted as $x_{[k]}$ for $k = 1, 2, \ldots, N$, where $\left|x_{[1]}\right| \leqslant \left|x_{[2]}\right| \leqslant \ldots \leqslant \left|x_{[N]}\right|$.

Both the correlation and Gini index suggest that the first mode is optimal, whereas the proposed methodology indicates that the third mode is optimal, as shown in Table 6 and Fig. 12.

Table 6. Analysis of mode properties: kurtosis, L-Kurtosis, correlation, and Gini index

| IMFs Measure | IMF1 | IMF2 | IMF3 | IMF4 | IMF5 |
|---|---|---|---|---|---|
| Kurtosis | 2.8172 | 3.2408 | **3.3399** | 3.0097 | 2.3660 |
| $\left|\Delta Lk\,(\text{IMFs})\right|$ | 3.4141 | 23.5075 | 0.3437 | 0.6756 | 4.1574 |
| Correlation | 0.6701 | 0.6621 | 0.4780 | 0.2553 | 0.1639 |
| Gini index | 1.0433 | 1.0401 | 1.0305 | 1.0164 | 0.9929 |
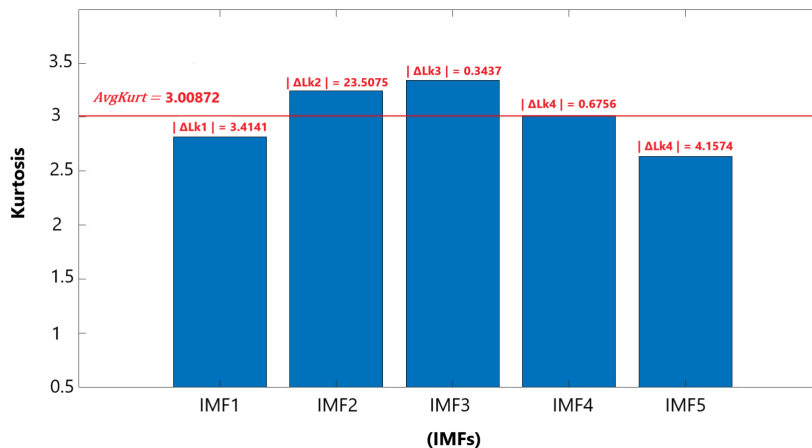


Fig. 12. Analysis of kurtosis and $\left|\Delta Lk\right|$ for each IMFs

Fig. 13 illustrates the envelope power spectra for each IMFs, showing results that demonstrate the superiority of the proposed methodology over correlation and Gini index indicators in detecting faults efficiently.

The results obtained using the proposed Variational Mode Decomposition methodology were compared to those obtained from Empirical Mode Decomposition into five modes. Frequency signals were extracted from the first three modes in each decomposition. Fig. 14 illustrates this comparison, highlighting the superior performance of the proposed VMD methodology in terms of information preservation and noise reduction. Additionally, Fig. 15 presents the power spectra of the envelope for the first three modes, demonstrating the enhanced effectiveness of our proposed methodology in extracting fault frequencies.
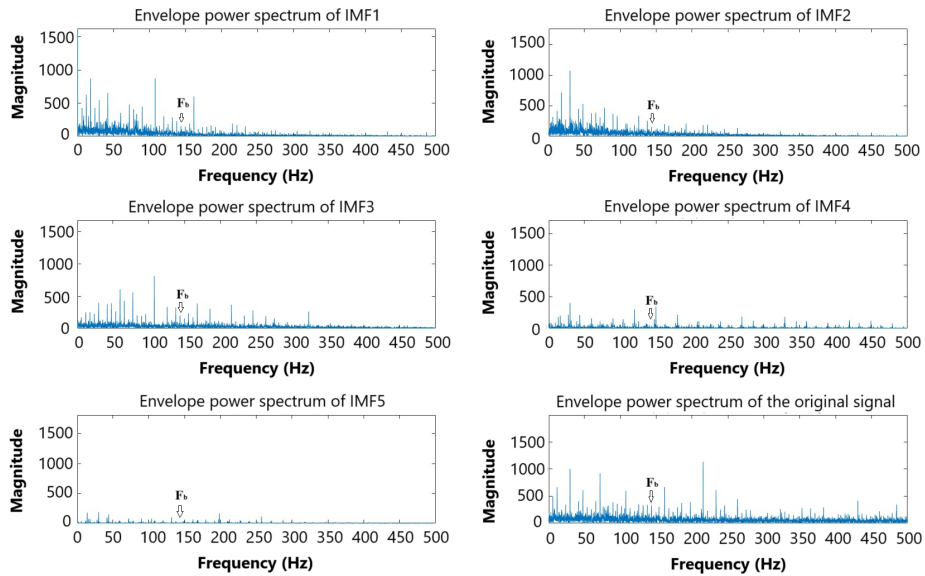
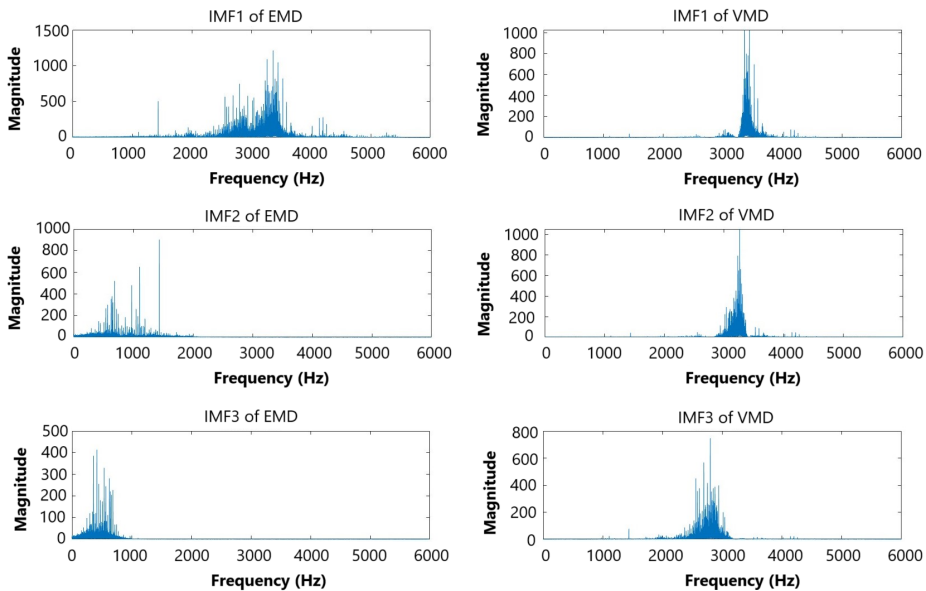Fig. 13. Frequency domain analysis



Fig. 14. Spectrum of IMF1-IMF3 after EMD and VMD

The results of this methodology are accurate, and faster compared to the studies mentioned in the literature that require the calculation of the frequency band over different window sizes.
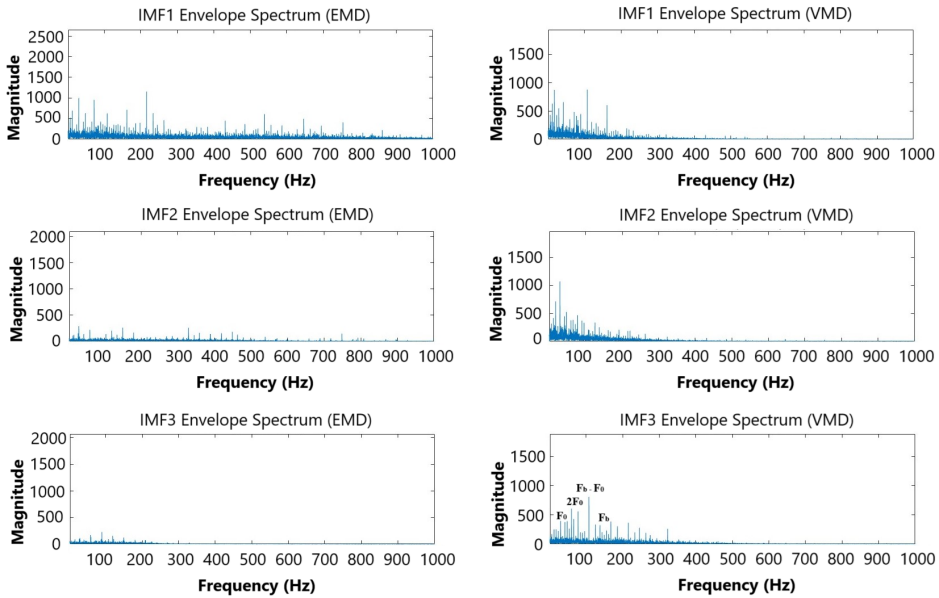
Fig. 15. Envelope spectrum of IMF1–IMF3 after EMD and VMD

### 3.3. XJTU-SY experimental dataset

The experiment was conducted on LDK UER204 bearings (Table 7) to diagnose an inner race wear fault. Two accelerometers of type PCB 352C33 were used, with one placed on the horizontal axis and the other on the vertical axis at a 90-degree angle. The testbed (Fig. 16) consists of an AC induction motor with a speed controller and a hydraulic loading system to apply the required radial force [22, 23].

Table 7. Summary table of characteristics

| Property | Value |
|---|---|
| Rotational speed | 2100 RPM (35 Hz) |
| Radial force | 12 kN |
| Sampling frequency | 25.6 kHz |
| Data points per sample | 32,768 data points |
| Recording duration per sample | 1.28 seconds |
| Sampling period | every 1 minute |
| Fault type | Inner Race Wear |
| Bearing type | LDK UER204 |

To calculate the Inner Race Fault Frequency (IRF), the formula (28) is used, where: $n = 8$ (number of balls), $d = 7.92$ mm (ball diameter), $D = 34.55$ mm
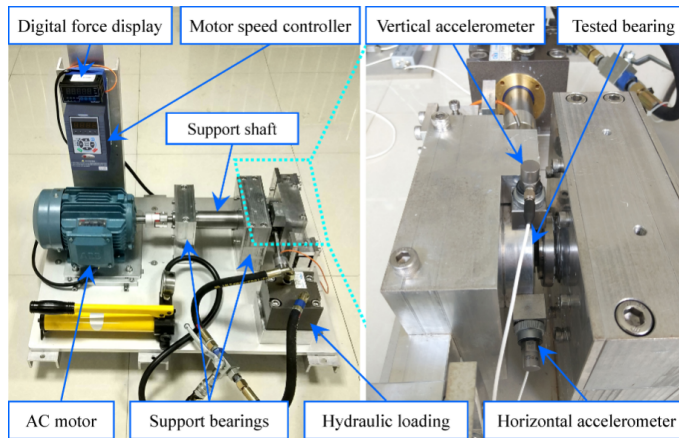
Fig. 16. Experimental setup of the XJTU-SY bearing testbed [23]

(pitch diameter), $\alpha = 0$ (contact angle), $fr = 35$ Hz (shaft rotational frequency).

$$f_{ir} = \frac{8}{2} \left( 1 + \frac{7.92}{34.55} \times 1 \right) \times 35 \approx 172.1 \text{ Hz}. \tag{33}$$

Fig. 17 displays the original horizontal and vertical fault signals before processing in the time and frequency domains, as well as the envelope and envelope spectrum.
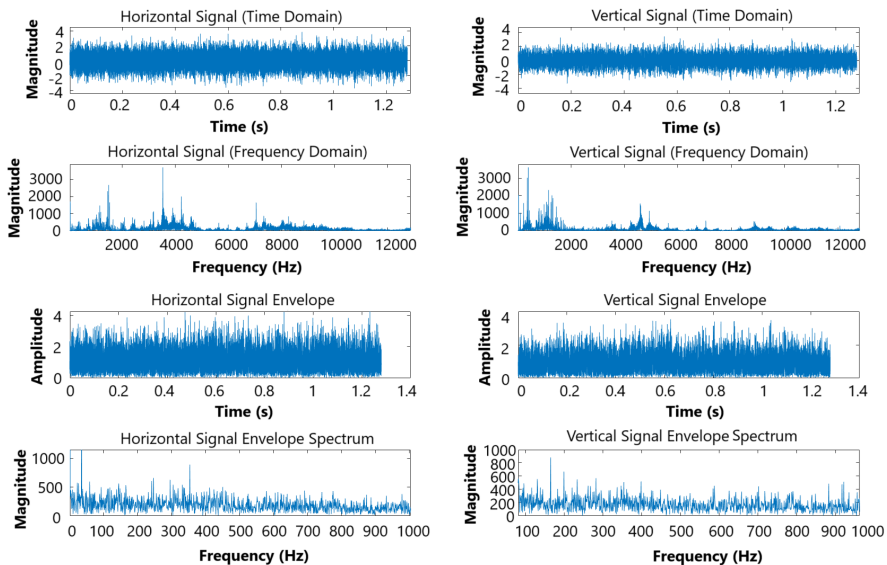


Fig. 17. Time domain, frequency domain, envelope, and envelope spectrum for horizontal and vertical faulty signals

Then, we determine the optimal alpha value according to our proposed method-ology:

- We obtain alpha = 1200 for the horizontal signal, as shown in Fig. 18.
- We obtain alpha = 1500 for the vertical signal, as shown in Fig. 19.



Fig. 18. Change in $|\Delta Lk|$ as a function of alpha for horizontal signal
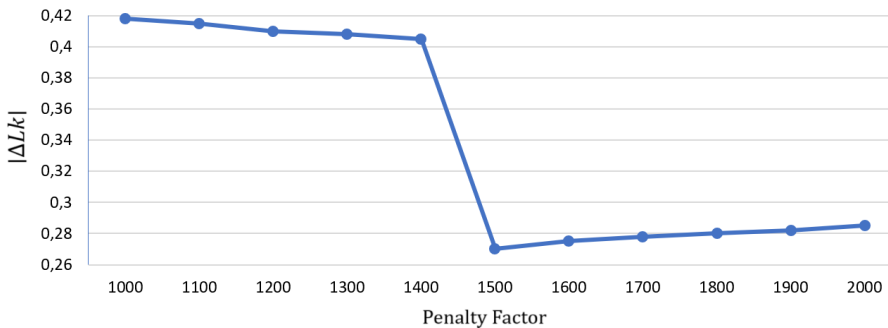


Fig. 19. Change in $|\Delta Lk|$ as a function of alpha for vertical signal

Determining the optimal $K$ for both signals is shown in Fig. 20 ($K = 5$ for the horizontal signal and $K = 8$ for the vertical signal).

Next, we extract the optimal modes:

- Fig. 21 shows the kurtosis values and the threshold for each intrinsic mode.
- Fig. 22 and Fig. 23 illustrate the envelope spectrum results for the extracted modes from both the horizontal and vertical signals.

Fig. 24 and Fig. 25 show a comparison between the results of VMD and EMD:

- We observe that the modes resulting from the improved VMD methodology provide a better distribution and more accurate fault frequency identification.
- Meanwhile, EMD concentrates most of the energy in the first four modes with lower accuracy compared to the improved VMD.

Based on Fig. 25, we observe that the fault frequency $Fi = 175$ Hz is clearly highlighted in IMF3, alongside the rotational frequency $F0$ and its second harmonic
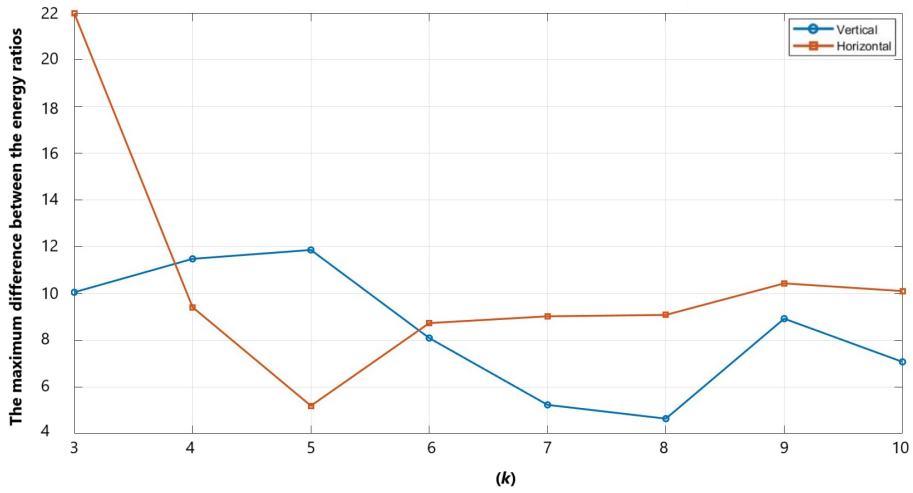
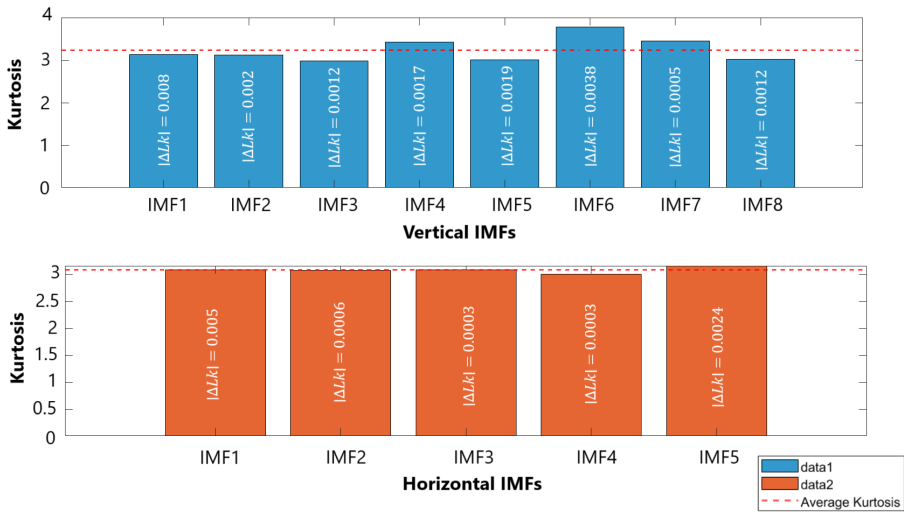Fig. 20. Evolution of the maximum difference between the energy ratios as a function of *K*



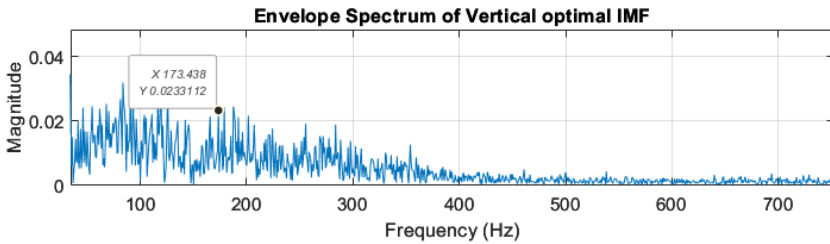Fig. 21. Kurtosis and $|\Delta Lk|$ for each IMFs (vertical and horizontal signals)



Fig. 22. Envelope spectrum of vertical IMF7
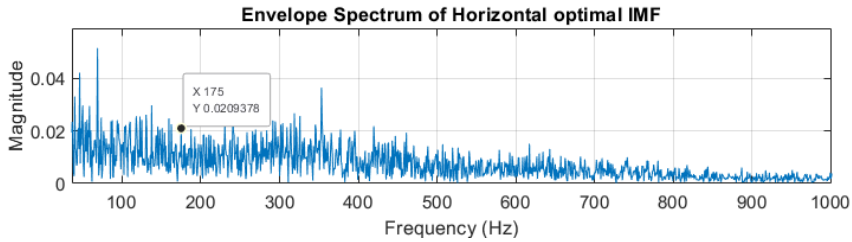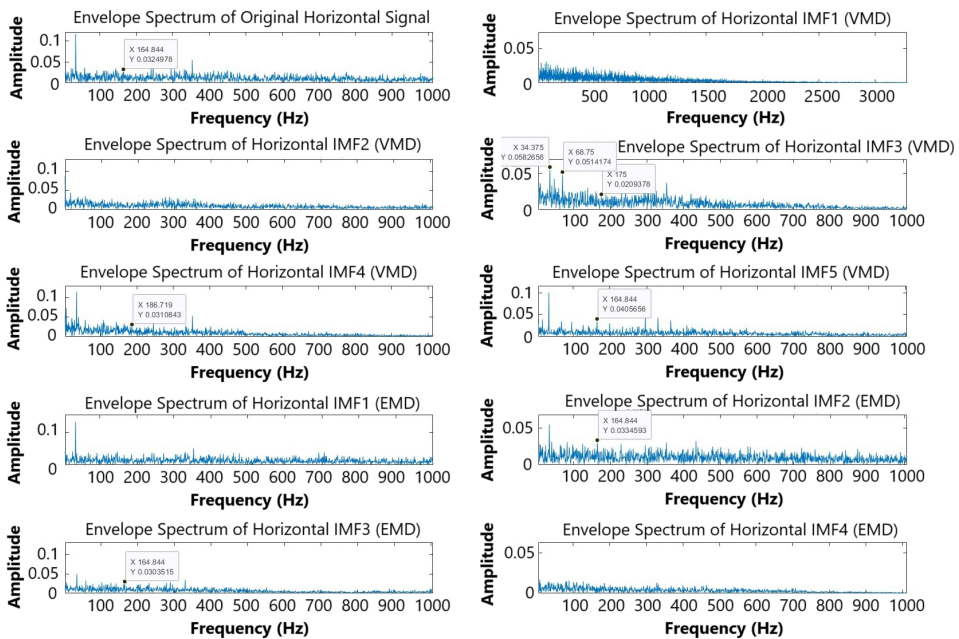
Fig. 23. Envelope spectrum of horizontal IMF3



Fig. 24. Comparative envelope spectrum analysis of VMD and EMD IMFs for the horizontal signal

$2F0$. In IMF5, which exhibits the highest kurtosis, the frequency $F = 164.8$ Hz emerges with an error of approximately 7.3 Hz. In contrast, using the EMD method, the frequency $F = 164.8$ Hz is detectable, but with less accuracy compared to the improved VMD, and no fault frequency with better accuracy is observed in EMD.

For the horizontal signal, the proposed VMD demonstrates a more diverse distribution and effectively identifies the fault frequency $Fi = 173.4$ Hz in IMF7. Additionally, $Fi = 164.8$ Hz is observed in IMF6, which has the highest kurtosis. However, in the EMD case, the 164.8 Hz frequency is not clearly visible, and the 170.3 Hz frequency shows a greater error compared to 173.4 Hz.
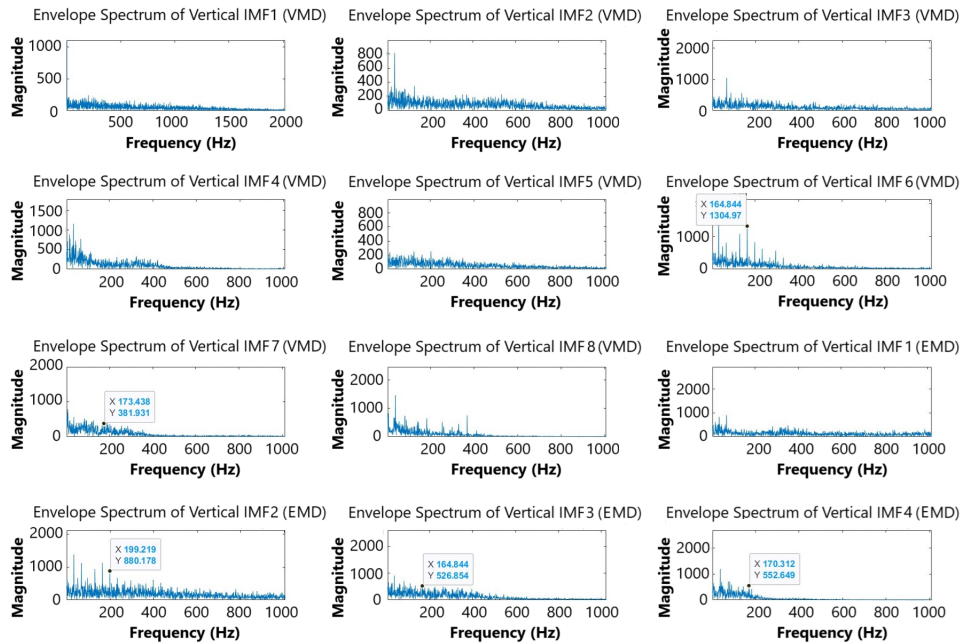
Fig. 25. Comparative envelope spectrum analysis of VMD and EMD IMFs for the vertical signal

## 3.4. Analysis of wind turbine bearing fault using the proposed approach

Wind turbines operate in a complex environment due to the constant variation in wind speed and its effects on different parts of the turbine. In this study, the focus will be on analyzing bearing characteristics and diagnosing potential faults using the following data [24]:

- High-Speed Shaft Speed Variation: The instantaneous speed of the shaft ranges from 30.9 Hz to 32.01 Hz, reflecting a speed variation of 3.6%.
- Bearing Fault Rates:
  - Cage Fault Rate: 0.42;
  - Ball Fault Rate: 2.87;
  - Inner Race Fault Rate: 9.46;
  - Outer Race Fault Rate: 6.72.

Analysis Data:

Fifty signals were measured to track the development of an inner race bearing fault, with the signal from day 45 (April 20) being taken as a reference (Fig. 26). These data from the reference (updated on 2018) [24, 25] will be used to diagnose the bearing fault.
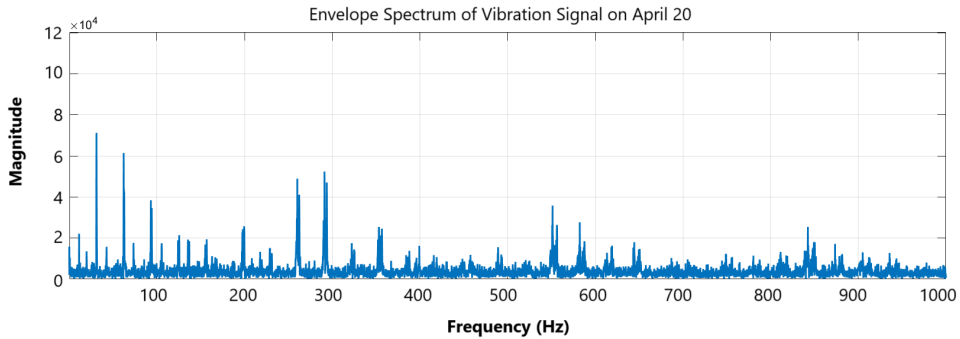
Fig. 26. Envelope power spectrum of the original signal

### 3.4.1. Selecting the optimal alpha using the proposed algorithm

- Input the original signal: let $x(t)$ be the original signal.
- Compute the L-Kurtosis of the original signal: $Lk_{\text{original}} = 0.8934$.
- Define parameters: number of components $K = 5$, range of $\alpha$ values: $\alpha \in [1000, 2000]$, set the initial $\alpha$ to 1000.
- Iterative VMD process: perform VMD: apply VMD to $x(t)$ with the current value of $\alpha$ to obtain IMFs.

Based on the results (Table 8), the optimal value of $\alpha$ is $\alpha = 1000$. This is because it yields the L-Kurtosis $Lk(\text{IMF}_{\text{max\_energy}}) = 0.6064$, which is the closest to the original L-Kurtosis $Lk_{\text{original}} = 0.8934$.

Table 8. Computed L-Kurtosis values

| $\alpha$ | $Lk(\text{IMF}_{\text{max\_energy}})$ |
|---|---|
| 1000 | 0.6064 |
| 1100 | 0.5647 |
| 1200 | 0.5283 |
| 1300 | −6.1442 |
| 1400 | −7.3411 |
| 1500 | −8.6192 |
| 1600 | −8.8045 |
| 1700 | −7.9415 |
| 1800 | −6.7761 |
| 1900 | −5.2002 |
| 2000 | −4.3810 |

### 3.4.2. Determining optimal $K$ and selecting the optimal IMF

We set $K$ values from 5 to 10; the stored $K$ and $\Delta E_{\text{max}}$ are described in the Table 9.

Table 9. Computed ($\Delta E_{\max}$) values

| $K$ | 5 | **6** | 7 | 8 | 9 | 10 |
|---|---|---|---|---|---|---|
| $\Delta E_{\max}$ | 0.1888 | **0.1078** | 0.1462 | 0.1528 | 0.1607 | 0.1598 |

Upon determining the appropriate number of modes, we perform the VMD with the specified parameters.

$$\left[\text{IMFs} + \text{res}\right] = \text{VMD}(x\,[n]\,1000\,,\,6). \tag{34}$$

Then we calculate the features (kurtosis, average kurtosis, L-Kurtosis, correlation, Gini index) for each mode, as illustrated in Table 10. Following this we will evaluate the results of selecting the optimal mode for each method.

Table 10. Measured characteristics of each IMFs

| IMFs<br>Measure | IMF1 | IMF2 | IMF3 | IMF4 | IMF5 | IMF6 |
|---|---|---|---|---|---|---|
| Kurtosis | 3.429 | 3.761 | 5.307 | 4.918 | 3.022 | 2.945 |
| Average kurtosis | 3.8975 | | | | | |
| L-Kurtosis | 0.891 | -1.582 | -5.984 | -1.012 | -0.870 | -3.025 |
| Correlation | 0.340 | 0.427 | 0.6378 | 0.563 | 0.348 | 0.372 |
| Gini index | 1.372 | 1.410 | 1.653 | 1.544 | 1.251 | 1.289 |

We observe that both IMF3 and IMF4 exceed the mean, while the L-Kurtosis value for the original signal is 0.8934. Therefore, we select IMF4 for fault detection.

Fig. 27 represents the envelope spectrum for the third and fourth modes. It is noted that the significant peak value in mode four corresponds to the fault frequency ($Fi$).
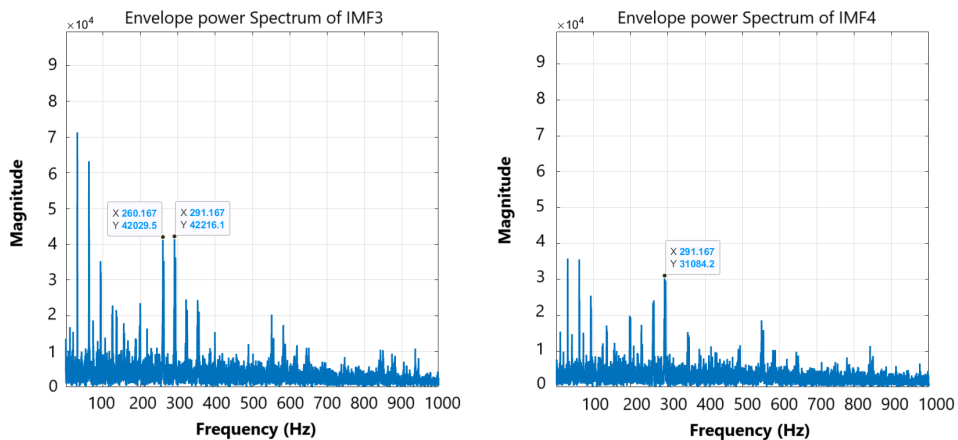


Fig. 27. Envelope spectrum of IMF3–IMF4

# 4. Conclusions

This paper presents an advanced approach for diagnosing bearing faults in wind turbines and rotating machinery using VMD. The proposed methodology focuses on optimizing the penalty factor in the VMD process and selecting the most relevant modes based on L-Kurtosis, kurtosis, and energy criteria. The goal is to enhance the detection accuracy of fault frequencies and reduce noise, making the approach suitable for real-time monitoring and fault diagnosis applications.

- CWRU Dataset:

For the inner race fault, the proposed VMD method identified the optimal mode as Mode 6, which exhibited a more pronounced fault frequency with higher amplitude in the envelope spectrum compared to other methods. Traditional correlation and kurtosis methods selected Mode 2 and Mode 7, respectively, but neither demonstrated the same level of fault frequency as clarity as the proposed approach.

In the ball fault experiment, the proposed methodology also outperformed Gini index and correlation methods, providing a clearer representation of the fault frequency in the envelope spectrum. The VMD method revealed more distinct peaks, enhancing the visibility of fault-related features.

Comparisons with the traditional Empirical Mode Decomposition method showed that the VMD method was more effective in fault detection and noise reduction. The VMD approach captured energy distribution more effectively, as indicated by the power spectra of the first three modes in the envelope spectrum, highlighting its superiority over EMD in preserving relevant information.

- XJTU-SY Dataset:

In the XJTU-SY dataset, the fault frequency of $Fi = 175$ Hz was clearly highlighted in IMF3, along with the rotational frequency $F0$ and its second harmonic $2F0$. Additionally, in IMF5, which exhibited the highest kurtosis, the frequency $F = 164.8$ Hz was observed with an error of approximately 7.3 Hz. In comparison, the EMD method detected the frequency $F = 164.8$ Hz with less accuracy and did not reveal other fault frequencies with better precision.

For the horizontal signal, the proposed VMD method demonstrated a more diverse distribution of fault frequencies, identifying $Fi = 173.4$ Hz in IMF7 and $Fi = 164.8$ Hz in IMF6, which had the highest kurtosis. In contrast, the EMD method struggled to accurately detect these frequencies, with significant errors in identifying fault frequencies, such as 170.3 Hz.

- Real-World Wind Turbine Fault Diagnosis:

For real-world inner race bearing fault diagnosis in wind turbines, all traditional indicators pointed to Mode 3 as the optimal mode for fault detection. However, the proposed VMD approach determined that Mode 4 was more suitable, as it exhibited the highest peak corresponding to the fault frequency in the envelope spectrum. This mode provided a clearer representation of the fault frequency, confirming its effectiveness in practical fault detection scenarios.

• Future Work:

The results of this study demonstrate the effectiveness of the proposed VMD methodology in bearing fault diagnosis, with significant improvements over traditional methods such as EMD, correlation, Gini index, and kurtosis. Future work will focus on developing new features based on this methodology to improve the accuracy of signal classification associated with different fault types. These features will aim to provide a more precise and deeper representation of signal patterns, thereby enhancing the diagnostic performance of classification systems in real-time applications.

## Acknowledgments

## References

[1] D. Meng, H. Wang, S. Yang, Z. Lv, Z. Hu, and Z. Wang. Fault analysis of wind power rolling bearing based on EMD feature extraction. *Computer Modeling in Engineering & Sciences*, 130(1):543–558. doi: 10.32604/cmes.2022.018123.

[2] M. Elgendi, M. AlMallahi, A. Abdelkhalig, and M.Y.E. Selim. A review of wind turbines in complex terrain. *International Journal of Thermofluids*, 17:100289, 2023. doi: 10.1016/j.ijft.2023.100289.

[3] D. Meng, S. Yang, A.M.P. de Jesus, and S. Zhu. A novel Kriging-model-assisted reliability-based multidisciplinary design optimization strategy and its application in the offshore wind turbine tower. *Renewable Energy*, 203:407–420, 2023. doi: 10.1016/j.renene.2022.12.062.

[4] D. Meng, H. Yang, S. Yang, Y. Zhang, A.M.P. de Jesus, J. Correia, T. Fazeres-Ferradosa, W. Macek, R. Branco, and S. Zhu. Kriging-assisted hybrid reliability design and optimization of offshore wind turbine support structure based on a portfolio allocation strategy. *Ocean Engineering*, 295:116842, 2024. doi: 10.1016/j.oceaneng.2024.116842.

[5] P. Santos, L.F. Villa, A. Reñones, A. Bustillo, and J. Maudes. An SVM-based solution for fault detection in wind turbines. *Sensors*, 15(3):5627–5648, 2015. doi: 10.3390/s150305627.

[6] S. Yang, Z. He, J. Chai, D. Meng, W. Macek, R. Branco, and S. Zhu. A novel hybrid adaptive framework for support vector machine-based reliability analysis: A comparative study. *Structures*, 58:105665, 2023. doi: 10.1016/j.istruc.2023.105665.

[7] J. Vives, J. Palací, and J. Heart. SVM-algorithm for supervision, monitoring and detection vibration in wind turbines. *Journal of Computer and Communications*, 10(11):44–55, 2022. doi: 10.4236/jcc.2022.1011004.

[8] F. Zhang, W. Sun, H. Wang, and T. Xu. Fault diagnosis of a wind turbine gearbox based on improved variational mode algorithm and information entropy. *Entropy*, 23(7):794, 2021. doi: 10.3390/e23070794.

[9] H. Peng, H. Zhang, Y. Fan, L. Shangguan, and Y. Yang. A review of research on wind turbine bearings' failure analysis and fault diagnosis. *Lubricants*, 11(1):14, 2023. doi: 10.3390/lubricants11010014.

[10] H. Li, T. Liu, X. Wu, and Q. Chen. An optimized VMD method and its applications in bearing fault diagnosis. *Measurement*, 166:108185, 2020. doi: 10.1016/j.measurement.2020.108185.

[11] M.G.A. Nassef, T.M. Hussein, and O. Mokhiamar. An adaptive variational mode decomposition based on sailfish optimization algorithm and Gini index for fault identification in rolling bearings, *Measurement*, 173:108514, 2021. doi: 10.1016/j.measurement.2020.108514.

[12] B. Xu, F. Zhou, H. Li, B. Yan, and Y. Liu. Early fault feature extraction of bearings based on Teager energy operator and optimal VMD. *ISA Transactions*, 86:249–265, 2019. doi: 10.1016/j.isatra.2018.11.010.

[13] A. Dibaj, R. Hassannejad, M.M. Ettefagh, and M.B. Ehghaghi. Incipient fault diagnosis of bearings based on parameter-optimized VMD and envelope spectrum weighted kurtosis index with a new sensitivity assessment threshold. *ISA Transactions*, 114:413–433, 2021. doi: 10.1016/j.isatra.2020.12.041.

[14] H. Li, T. Liu, X. Wu, and Q. Chen. Application of optimized variational mode decomposition based on kurtosis and resonance frequency in bearing fault feature extraction. *Transactions of the Institute of Measurement and Control*, 42(3):518–527, 2020. doi: 10.1177/0142331219875348.

[15] K. Dragomiretskiy and D. Zosso. Variational mode decomposition. *IEEE Transactions on Signal Processing*, 62(3):531–544, 2014. doi: 10.1109/TSP.2013.2288675.

[16] A. Lakikza, H. Cheghib, and N. Kahoul. Diagnosis of bearing faults in wind turbine systems using vibrational signal processing and machine learning. *Diagnostyka*, 25(3):2024307, 2024. doi: 10.29354/diag/191393.

[17] A. Kumar, Y. Zhou, and J. Xiang. Optimization of VMD using kernel-based mutual information for the extraction of weak features to detect bearing defects. *Measurement*, 168:108402, 2021. doi: 10.1016/j.measurement.2020.108402.

[18] Z. Qiao, Y. Lei, and N. Li. Applications of stochastic resonance to machinery fault detection: A review and tutorial. *Mechanical Systems and Signal Processing*, 122:502–536, 2019. doi: 10.1016/j.ymssp.2018.12.032.

[19] S. Liu, S. Hou, K. He, and W. Yang. L-Kurtosis and its application for fault detection of rolling element bearings. *Measurement*, 116:523–532, 2018. doi: 10.1016/j.measurement.2017.11.049.

[20] H. Liu and J. Xiangi. A strategy using variational mode decomposition, L-Kurtosis and minimum entropy deconvolution to detect mechanical faults. *IEEE Access*, 7:70564-70573, 2019. doi: 10.1109/ACCESS.2019.2920064.

[21] Vibration Database. Case Western Reserve University, 2024. https://engineering.case.edu/bearingdatacenter/download-data-file

[22] XJTU-SY Bearing Dataset for Fault Diagnosis, [Online]. Available: https://biaowang.tech/xjtu-sy-bearing-datasets/

[23] B. Wang, Y. Lei, N. Li, and N. Li. A hybrid prognostics approach for estimating remaining useful life of rolling element bearings. *IEEE Transactions on Reliability*, 69(1):401–412, 2020. doi: 10.1109/TR.2018.2882682.

[24] E. Bechhoefer, B. Van Hecke, and D. He. Processing for improved spectral analysis. *Annual Conference of the Prognostics and Health Management Society*, New Orleans, USA, 2013. doi: 10.36001/phmconf.2013.v5i1.2220.

[25] The data is available on this website: https://github.com/mathworks/WindTurbineHighSpeedBearingPrognosis-Data